Journal of Molecular Structure 1181 (2019) 312–320

Contents lists available at ScienceDirect

Journal of Molecular Structure

journal homepage: http://www.elsevier.com/locate/molstruc

Effect of gold nanoparticle shape on the photophysicochemical properties of sulphur containing metallophthalocyanines

Edith Dube, Tebello Nyokong*

Center for Nanotechnology Innovation, Department of Chemistry, Rhodes University, Grahamstown 6140, South Africa

ARTICLE INFO

Article history:
Received 29 October 2018
Received in revised form
7 December 2018
Accepted 23 December 2018
Available online 26 December 2018

Keywords:
Gold nanotriangles
Benzothiazole
Thiophene ethoxy
Metallophthalocyanines
Singlet oxygen quantum yield

ABSTRACT

In this work tetrakis–[(thiopheneethoxy) phthalocyaninato] zinc(II) (**1**), tetrakis–[(thiopheneethoxy) phthalocyaninato] indium (II) chloride (**2**), tetrakis [(benzo [*d*]thiazol-2-yl phenoxy) phthalocyaninato] zinc(II) (**3**), and tetrakis [(benzo [*d*]thiazol-2-yl phenoxy)phthalocyaninato] indium (II) chloride (**4**) were linked to both gold nanospheres (AuNSs) and gold nanotriangles (AuNTs) via Au-S and Au-N (the latter for complexes **3** and **4** only) self assembly. The photophysicochemical behaviour of complexes and their conjugates were studied. The conjugates yielded improved triplet and singlet quantum yields, with nanospheres displaying better properties than nanotriangles. The conjugates with a benzothiazole phenoxy substituent also yielded better properties than their thiophene ethoxy counterpart. These conjugates especially those with a benzothiazole phenoxy substituent have potential as photosensitisers for photodynamic therapy applications.

1. Introduction

Metallophthalocyanines (MPcs) are photosensitisers (PS) characterised by high triplet quantum yields and lifetimes [1] depending on the nature of the central metal and ring substituents [2,3]. These properties consequently yield high singlet oxygen quantum yields making MPcs good candidates for photodynamic therapy (PDT). PDT is a clinically approved, minimally invasive cancer treatment which requires a PS and light of appropriate wavelength in the presence of ground state molecular oxygen to elicit selective destruction of cancer cells [1]. MPcs such as Photosens, Photocyanine and Pc4 are in clinical trials as PSs for PDT [4,5]. Even though successes are being recorded for the PDT activity of MPcs, some drawbacks which include limited selectivity and specificity of these PSs towards cancer cells in comparison to healthy ones still remain [6,7]. It has been shown that conjugation of the PS to nanoparticles leads to increased selectivity and specificity [8,9].

Cancer cells preferentially internalise nanoparticles due to the specific properties of tumours when compared to healthy tissue, a phenomenon called the enhanced permeability and retention (EPR) effect [10,11]. The uncontrolled and rapid growth of cancer cells leads to the formation of abnormal, leaky, disorganised and loosely-connected blood vessels with an increased vessel permeability due to pore sizes of about 100–600 nm compared to 10 nm in healthy tissue. Nanoparticles can easily permeate through tumour vasculature and once nanoparticles have been internalised, they will be retained due to the inability of tumours to renew and clean the interstitial fluid [11–14].

The shape and size of a nanoparticle linked to MPcs governs the latter's *in vivo* journey and destination dictating its biodistribution, targeting, uptake and circulation time in tumour cells [15,16]. A high cellular uptake has been reported for spherical gold nanoparticles compared to anisotropic counterparts, however the anisotropic nanoparticles are generally reported to have a higher circulation time [17–19]. The triangular shaped nanoparticles on the other hand have shown better cellular uptake compared to other anisotropic nanoparticles (order of cellular uptake efficiency: triangles > rods > stars) [20], hence the interest in nanoparticle shape in this work.

In this work symmetric MPcs containing zinc and indium as central metals, with benzothiazole phenoxy and thiophene ethoxy as substituents are linked to gold nanospheres (AuNSs) and gold nanotriangles (AuNTs) for the first time. The effect of nanoparticle shape, the central metal and that of substituents on the photophysicochemical properties will be explored.

MPcs with In and Zn were chosen because they result in high triplet state quantum yields through the heavy atom effect, which

* Corresponding author.
E-mail address: t.nyokong@ru.ac.za (T. Nyokong).

https://doi.org/10.1016/j.molstruc.2018.12.091
0022-2860/

promotes intersystem crossing to populate the triplet state [21]. The benzothiazole phenoxy and thiophene ethoxy substituents on the other hand, were chosen since both the benzothiazole and thiophene derivatives have been found to have antitumor activities [22–26] and this could be advantageous for PDT applications. Both substituents have a thiol group which can easily interact with gold nanoparticles.

2. Experimental

Materials and equipment employed are detailed in Supporting Information.

2.1. Linkage of complexes 1–4 to nanoparticles (Scheme 2)

The syntheses of tetrakis–[(thiopheneethoxy) phthalocyaninato] zinc(II) (**1**) [27], tetrakis–[(thiopheneethoxy) phthalocyaninato] indium (II) chloride (**2**) [28], tetrakis [(benzo [*d*]thiazol-2-yl phenoxy) phthalocyaninato] zinc(II) (**3**) [29], tetrakis [(benzo [*d*] thiazol-2-yl phenoxy)phthalocyaninato] indium (II) chloride (**4**) [30], tetraoctylammonium bromide (TOAB) capped gold nanospheres (AuNSs) [31], and hexadecyltrimethylammonium chloride (CTAC) capped gold nanotriangles (AuNTs) [32] have been previously reported in literature.

For the synthesis of the phthalocyanine–NPs conjugates complex **1** (0.020 g, 0.019 mmol), complex **2** (0.020 g, 0.017 mmol), complex **3** (0.020 g, 0.014 mmol), and complex **4** (0.02 g, 0.013 mmol) were separately dissolved in dry dimethyl formamide (DMF, 2 mL). Then AuNSs (0.5 mg in 3 mL toluene) were added and the reaction mixture was stirred for 24 h at room temperature. The same procedure was followed for AuNTs. The conjugates were centrifuged, successively washed with ethanol and allowed to dry in the fume hood. The conjugates are represented as **1**-AuNSs, **1**-AuNTs, **2**-AuNSs, **2**-AuNTs, **3**-AuNSs, **3**-AuNTs, **4**-AuNSs and **4**-AuNTs.

2.2. Photophysicochemical studies

Fluorescence (Φ_F) and triplet (Φ_T) quantum yields were determined in DMSO using comparative methods described before in literature [33,34]. Unsubstituted ZnPc in DMSO was used as a standard with $\Phi_F = 0.20$ [34] and $\Phi_T = 0.65$ [33]. The solutions for triplet state studies were de-aerated with argon for 15 min before measurements.

Singlet oxygen quantum yield ($\boldsymbol{\Phi_\Delta}$) values were determined under ambient conditions using 1,3-diphenylisobenzofuran (DPBF) as a singlet oxygen quencher in dimethylsulfoxide (DMSO), and anthracene-9,10-bis-methylmalonate (ADMA) in water, and calculated using equations already described before [35,36]. Unsubstituted ZnPc in DMSO was used as a standard ($\Phi_{\Delta(Std)} = 0.67$ in DMSO) [35]. AlPcSmix (containing a mixture of differently substituted phthalocyanines) was employed as a standard in aqueous media ($\Phi_{\Delta(Std)} = 0.42$ [37]. The absorbances of DPBF or ADMA were spectroscopically monitored at 417 nm or 380 nm, respectively, at predetermined time intervals.

3. Results and discussion

Schemes 1 and 2, show the linkage of the Pcs to gold nanotriangles using complex **1** and **2** as examples, and to gold nanospheres using complex **3** and **4** as examples. Complexes **1**–**4** were each self-assembled to both AuNTs and AuNSs using the Au-S or Au-N interactions (the latter for complexes **3** and **4** only).

3.1. Characterization

3.1.1. Electronic absorption spectra of Pc complexes and their conjugates

Fig. 1A, shows an overlay of the normalised absorption spectra of AuNTs and AuNSs. The AuNSs are characterised by a surface plasmon resonance peak at 526 nm, while AuNTs show two bands at 609 nm and 570 nm, attributed to the in-plane dipole and out-of-plane dipole resonance of gold nanoplates, respectively, characteristic of AuNTs [38].

The electronic ground state absorption spectra of the conjugates of complexes **1**–**4** with both AuNTs and AuNSs are shown in Fig. 1B and C, with some in Fig. S1 A and B, ESI†. The Pcs alone and conjugates showed a typical electronic spectra with two strong absorption regions, in the UV region between 300 and 400 nm (B band) and in the visible region between 600 and 750 nm (Q band) [39]. The red shift in the Q band of complexes **2** and **4** compared to corresponding **1** and **3** (Table 1), can be attributed to the non-planar effect of the indium (III) ion, with a relatively bigger atomic radius than the zinc(II) ion as the central metal ion in the Pc cavity [40]. The enhanced absorption of the conjugates between the 400–600 nm regions, confirms the presence of gold nanoparticles (AuNTs and AuNSs). The MPcs alone are generally characterised by minimum to no absorption within this region. The conjugates with thiophene ethoxy substituents are slightly red shifted compared to their benzothiazole phenoxy counterparts, Table 1. This is in line with their respective Pc complexes when alone.

The Pc and their conjugates are insoluble in water, hence for

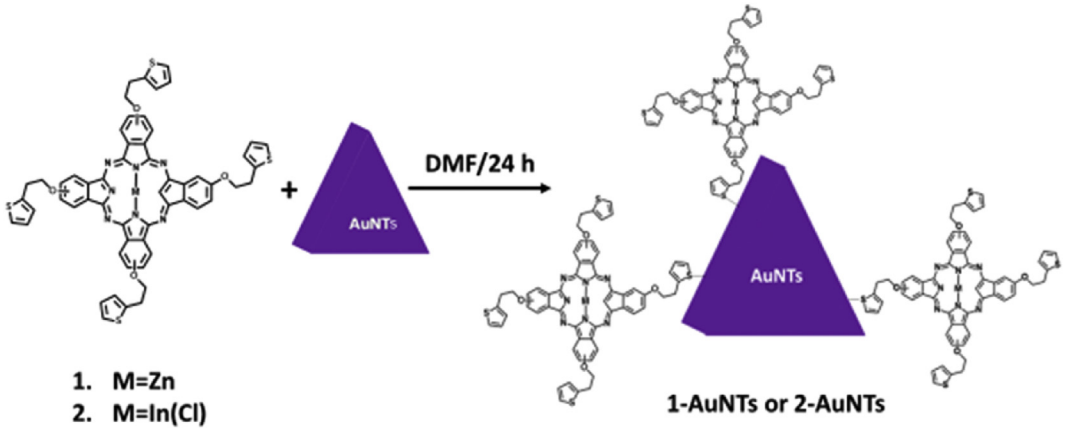

Scheme 1. Synthetic pathways for **1**-AuNTs and **2**-AuNTs.

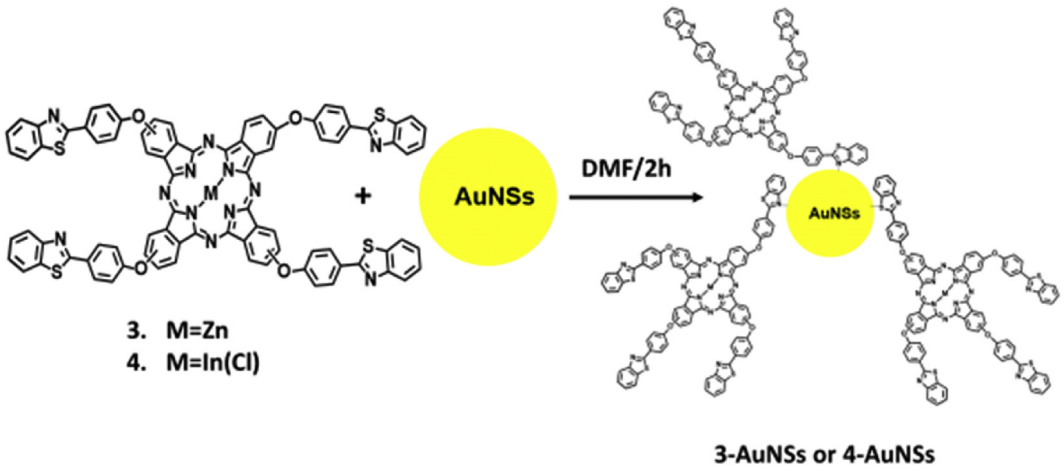

Scheme 2. Synthetic pathways for **3**-AuNSs and **4**-AuNSs.

studies in water they were first dissolved in 50 μL DMSO and then diluted with water to 5 mL (1% (v/v) DMSO in water). Studies in aqueous media are important for biological applications especially in PDT. The MPcs alone and their conjugates (Fig. S2, ESI†) were extensively aggregated in water (containing 1% DMSO) as shown by broadened Q bands. Aggregation in Pcs is attributed to π–π stacking interactions of the aromatic rings of Pcs [39]. The loading of complexes **1** to **4** onto the nanoparticles was investigated following literature methods [41]. Briefly this involved comparing the Q band absorbance intensity of the MPc in the conjugate with that of the MPc before conjugation. The loading values are shown in Table 1. The loading for AuNTs was less compared to that of AuNSs. This could be due to the plate like nature of these nanotriangles (also termed nanoplates) that tends to stack on each other face-to-face or edge to edge [42] in addition to the large edge length (52.7 nm, from TEM to be discussed below). This reduces the loading capacity of the nanoparticles. The loading capacity is greatly influenced by the nanoparticle surface area [43], which in this case is greatly affected by the particle size and aggregation [44]. The small AuNS size could be the reason for the high loading compared to the relatively large AuNTs.

An overlay of the normalised emission, excitation and absorption spectra of **1**-AuNSs is shown in Fig. 2, as an example. The ground state electronic absorption and excitation spectra of Pcs are usually similar, however the slight differences observed in the conjugates are attributed to the absorbance by the gold nanoparticles in the conjugate. The emission spectra were mirror images of the excitation spectra as expected.

3.1.2. TEM images

The TEM micrographs and the size distribution bar graphs of AuNTs and AuNSs are shown in Fig. 3. The nanoparticles appear mostly monodispersed. The edge length of AuNTs was averaged to 52.7 nm and the AuNSs had an average diameter of 15.2 nm. Upon conjugation of the NPs to complexes there was considerable aggregation. Aggregation upon conjugation could be due to π-π interaction from adjacent Pcs [39].

3.1.3. XRD studies

Fig. 4 shows the powder XRD patterns of AuNSs, **1**-AuNSs and **2**-AuNSs which were used as examples. The NPs and their conjugates displayed a powder diffraction pattern resembling a face centered cubic crystal (FCC) structure, characteristic of metallic gold. Well-defined crystalline peaks at 2θ = 38.2, 44.1, 63.9, 77.1 and 81.1°, assigned to the 111, 200, 220, 311 and 222 planes characteristic of gold [45] were observed (Fig. 4), confirming its presence. Also observed were broad peaks between 2θ = 12–22° in the conjugates, characteristic of the amorphous nature of phthalocyanines [46] confirming their presence. The Debye-Scherrer equation (1) [47], was employed for the estimation of the size of the AuNSs:

$$d = \frac{k\lambda}{\beta\cos\theta} \quad (1)$$

where λ is the wavelength of the X-ray source (1.5405 Å), k is an empirical constant equal to 0.9, β is the full width at half maximum of the diffraction peak and θ is the angular position. The sizes (diameter) were estimated to be 14.9 nm (AuNSs), 17.7 nm (**1**-AuNSs), 17.2 nm (**2**-AuNSs), 16.9 nm (**3**-AuNSs), 17.6 (**4**-AuNSs). There is an increase in the size of the NPs upon coordination to the Pcs, probably due to aggregation as discussed above.

3.1.4. EDX spectra

The elemental compositions of the nanoparticles, MPcs and conjugates were qualitatively determined using an energy dispersive X-ray spectrometer (EDX) and Fig. 5 shows the spectra for AuNSs, **3**-AuNSs and **4**-AuNSs as examples. The NPs alone showed the presence of C and Au (the carbon is from the capping agent), while all conjugates showed C, N, O, S, Au in addition to their respective central metals, that is Zn for the zinc conjugate and indium together with chlorine for the indium conjugate.

3.1.5. XPS spectra

The possible interaction between nanoparticles and complexes was assessed using high resolution XPS analysis, using complex **3** and **3**-AuNTs as examples. The Pc complexes alone were deconvoluted into two peaks (using complex **3** alone as an example) for both the S 2p and N 1s, corresponding to –S–C– (161.9 eV), –S– (163.0 eV) (Fig. 6A), –N–C– (396.2eV) and –N– (397.3 eV), Fig. S3A, ESI†. The conjugates were deconvoluted into three peaks (using **3**-AuNTs as an example), attributed to –S–C– (161.8 eV), –S– (163.0 eV), –S–Au– (166.7 eV) for the S 2p (Fig. 6B), –N–C– (396.2eV), –N– (397.5eV) and –N–Au– (402.9 eV) for the N 1s peak (Fig. S3B, ESI†). The S-Au and N-Au peaks indicate the successful linkage of complexes to nanopaticles via S-Au and N-Au interactions.

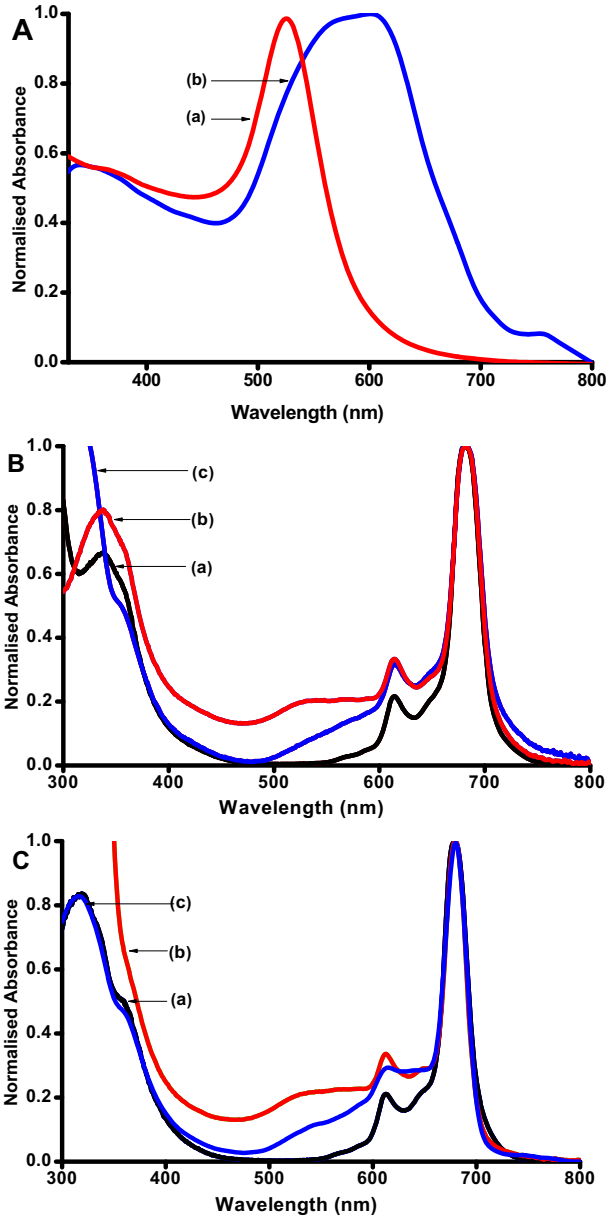

Fig. 1. UV–vis absorption of (A) AuNSs (a) and AuNTs (b); (B) complex **1** (a), **1**-AuNSs (b), **1**-AuNTs (c); and (C) complex **3** (a), **3**-AuNSs (b), **3**-AuNTs (c) in DMSO.

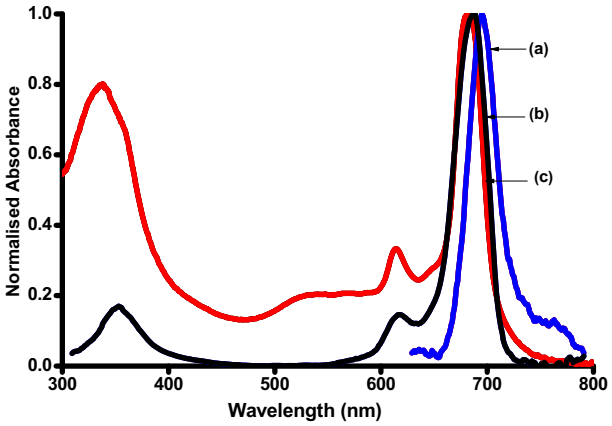

Fig. 2. Emission (a), excitation (b) and absorption (c) spectra of **1**-AuNSs (excitation = 610 nm, solvent = DMSO).

3.2. Photophysicochemical parameters

The fluorescence quantum yields (Φ_F) and lifetimes (τ_F), triplet quantum yields (Φ_T) and lifetimes (τ_T), as well as singlet oxygen quantum yields (Φ_Δ) in DMSO for complexes **1**–**4** alone (from literature) [28,30] and after conjugation with AuNTs and AuNSs are shown in Table 1. The singlet oxygen quantum yields (Φ_Δ) was also determined in water (containing 1% DMSO) and the values are also indicated in Table 1.

3.2.1. Fluorescence quantum yields (Φ_F) and lifetimes (τ_F)

The indium atom quenches the fluorescence lifetime and lowers the fluorescence quantum yield of Pcs more than is the case with the zinc atom as shown by very low values of Φ_F and τ_F, for complexes **2** and **4** and their conjugates, Table 1. This is attributed to the heavy atom effect since indium is heavier than zinc. Linkage to AuNSs and AuNTs resulted in reduction in Φ_F of the Pcs (Table 1), as expected due to the heavy atom effect of gold, which promotes intersystem crossing to the triplet state thus reducing fluorescence.

The shape and size of the nanoparticles seems to have an effect on the fluorescence behaviour of dyes. For complexes **1** and **3**, the conjugates to nanospheres displayed low Φ_F compared to their nanotriangle counterparts. This may be attributed to the smaller size of the AuNSs (15.2 nm, diameter) compared AuNTs (52.7 nm, edge length). Smaller NPs have been shown to exhibit a greater fluorescence quenching effect [48]. Additionally, nanospheres resulted in more loading of complexes than nanotriangles, Table 1,

Table 1
Photophysicochemical parameters of complexes 1–4 and their conjugates in DMSO.

Samples	Pc loading (μg/mg)	λ_{abs} (nm)	(Φ_F) (±0.01)	τ_F (ns) (±0.01)	τ_0(ns)	(Φ_T) (±0.02)	τ_T (μs) (±1.00)	Φ_Δ[b] (±0.01)
[a]**1**		682	0.15	3.12	20.8	0.47	306	0.33 (0.07)
1-AuNSs	37	682	0.08	2.92	36.5	0.61	202	0.46 (0.08)
1-AuNTs	24	681	0.12	2.98	24.8	0.53	214	0.39 (0.07)
[a]**2**		695	0.02	0.88	44.0	0.60	225	0.42 (0.08)
2-AuNSs	29	695	<0.01	0.55	–	0.70	78	0.60 (0.11)
2-AuNTs	17	694	<0.01	0.69	–	0.64	86	0.52 (0.09)
[a]**3**		679	0.17	3.08	18.1	0.59	149	0.50 (0.07)
3-AuNSs	22	680	0.14	2.63	18.8	0.68	188	0.56 (0.10)
3-AuNTs	19	679	0.16	2.87	17.9	0.62	199	0.53 (0.08)
[a]**4**		690	0.03	0.78	26.0	0.75	55	0.64 (0.12)
4-AuNSs	32	692	<0.01	0.49	–	0.86	67	0.74 (0.15)
4-AuNTs	20	693	<0.01	0.58	–	0.81	72	0.69 (0.13)

[a] Literature values [28,30].
[b] numbers in brackets are the values in water containing 1% DMSO (v/v).

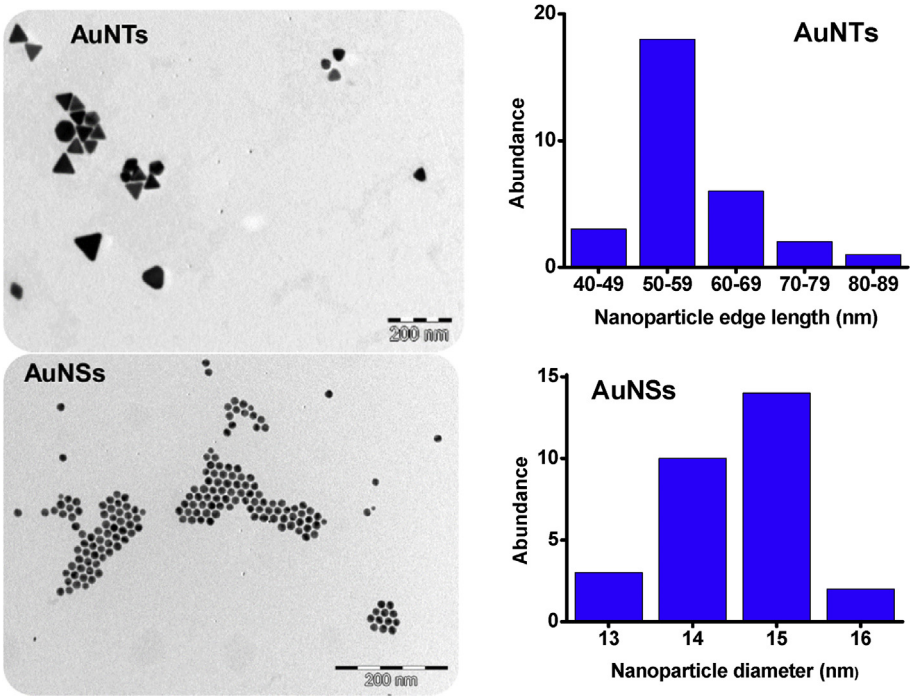

Fig. 3. Representative TEM micrographs and size distribution plots for AuNTs and AuNSs.

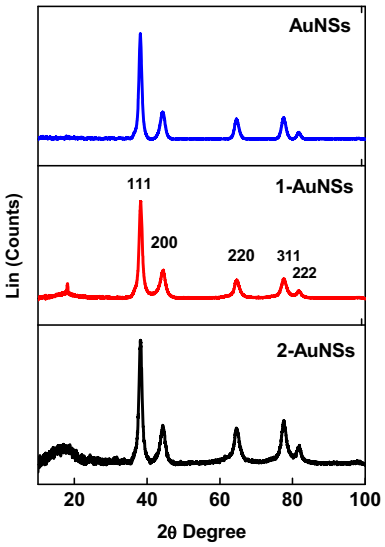

Fig. 4. XRD diffractograms for AuNSs, **1**-AuNSs, and **2**-AuNSs.

this could result in more aggregation. Aggregates are known to convert electronic excitation energy to vibrational energy which consequently decreases the fluorescence quantum yield of molecules [49]. It should be noted that MPcs can assume different conformations around the NPs. The distance or orientation between the fluorophore (MPc) and the metallic nanoparticles has been shown to have an effect on their fluorescence properties [50]. For **2** and **4**, the Φ_F values were too low to be compared.

The conjugates displayed a bi-exponential decay, hence existence of two lifetimes (Fig. 7, using **1**-AuNTs as example) and this could be due to different orientations of the MPcs on the NPs [51]. The average lifetimes for the conjugates are presented in Table 1. As expected the fluorescence lifetimes decreased with the decrease in Φ_F since the two have a direct relationship. Following the kinetic model, the excited state lifetimes are directly related to the radiative lifetime (τ_0) hence these were determined using the measured fluorescence quantum yield (Φ_F) and lifetime (τ_F) as shown in equation (2) [52,53].

$$\tau_0 = \frac{\tau_F}{\Phi_F} \tag{2}$$

With this model, increase in radiative lifetime will result in a corresponding increase in fluorescence lifetime and a decrease in fluorescence quantum yield. This suggests that a decrease in fluorescence quantum yield can be significantly higher than the corresponding fluorescence lifetime. Indeed, all the complexes and the corresponding conjugates having high radiative lifetime showed lower fluorescence quantum yield (Table 1) in accordance with the model.

3.2.2. *Triplet quantum yields (Φ_T) and lifetimes (τ_T)*

A representative transient curve of the conjugate **1**-AuNTs (as an example) is shown in Fig. 8A. All complexes and conjugates showed a negative absorption in the Soret and Q band region, attributed to the depletion of the phthalocyanine ground state. A broad positive absorption centered near 500 nm was attributed to the triplet-triplet absorption ($T_1 \rightarrow T_n$) [54].

The triplet state quantum yield (Φ_T) is an important property of MPcs for application in PDT. It represents the fraction of molecules that undergoes intersystem crossing to the triplet excited state and this greatly influences the singlet oxygen production. Fig. 8B, shows the triplet decay curve of the conjugate **1**-AuNSs (as an example). The triplet decay curve obeyed second order kinetics, typical of MPc complexes at high concentration, due to triplet–triplet recombination [55].

Complexes **2** and **4** displayed much larger Φ_T values compared to the corresponding complexes **1** and **3** due the differences in the central metal. Indium a heavier atom than zinc results in comparatively faster intersystem crossing to the triplet state due to the

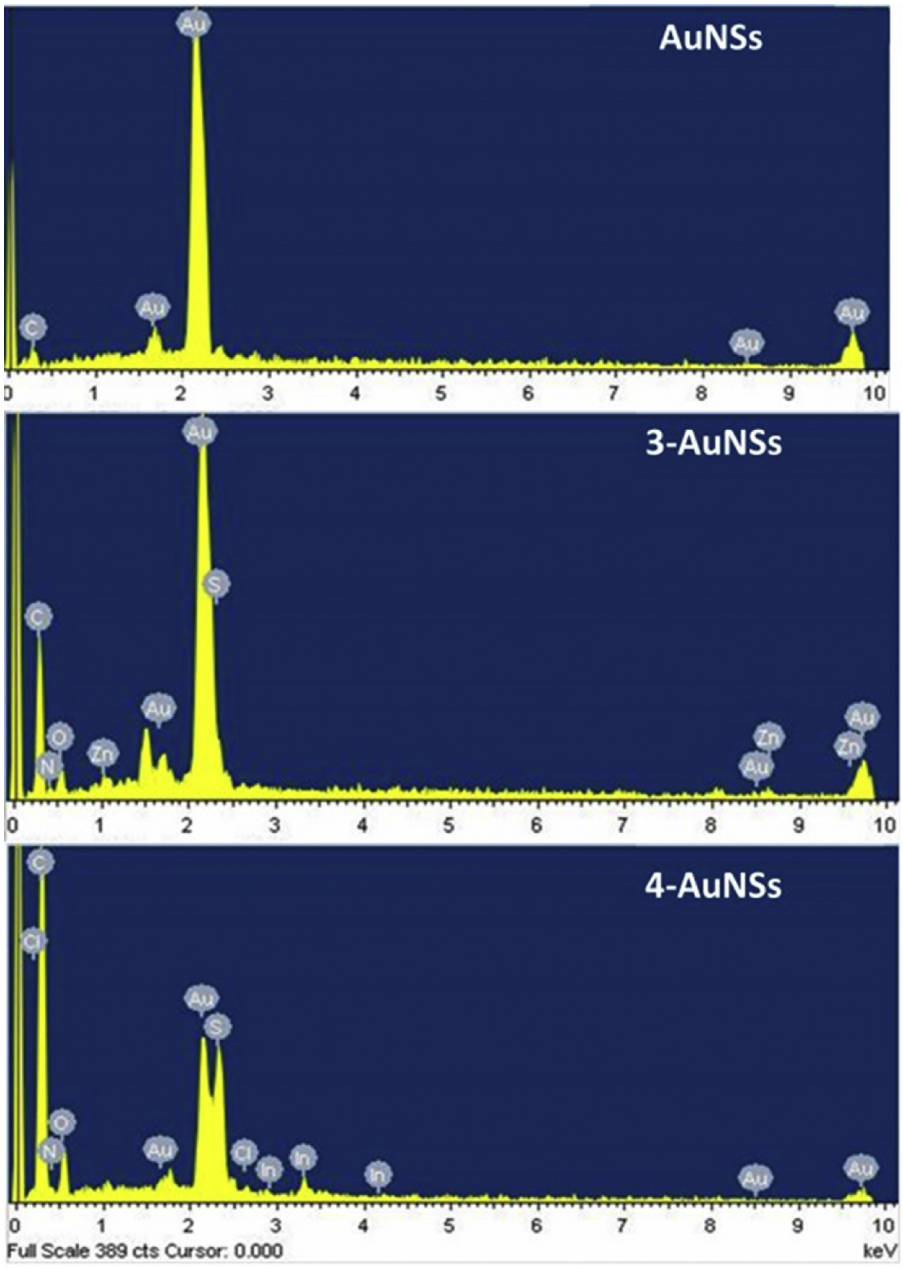

Fig. 5. EDX spectra for AuNSs, **3**-AuNSs and **4**-AuNSs.

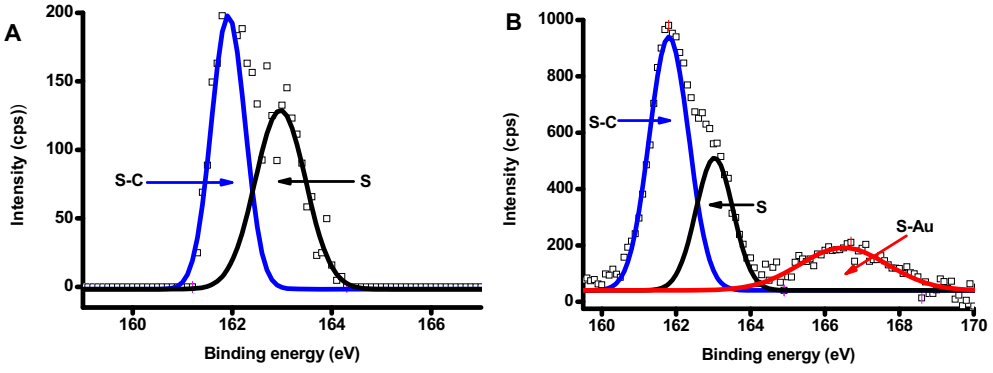

Fig. 6. XPS high resolution S 2p spectra for (A) complex **3** and (B) S 2p for **3**-AuNTs.

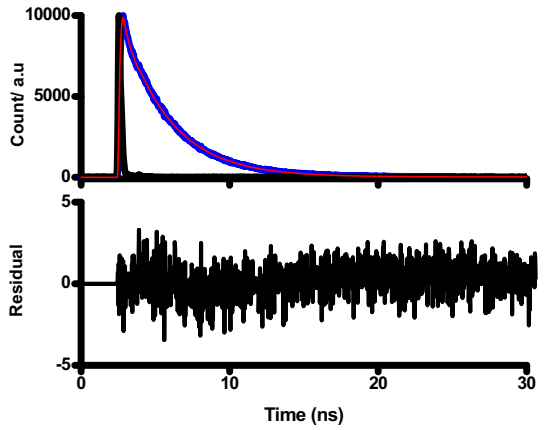

Fig. 7. Fluorescence decay (blue), χ^2 fitting (red) and IRF (black) curves for complex **1**-AuNTs in DMSO.

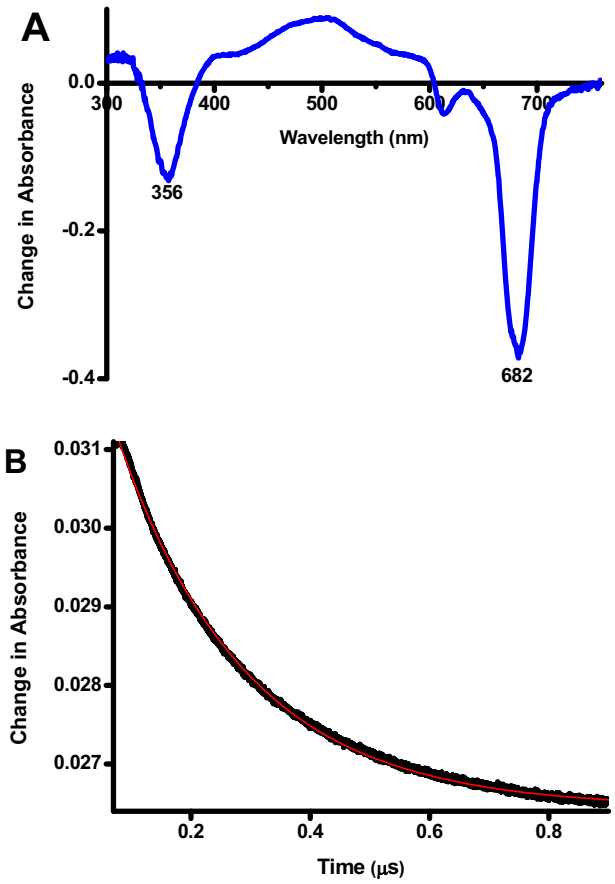

Fig. 8. (A) Transient curve and (B) triplet absorption decay curve (black) and fitting (red) for **1**-AuNSs in DMSO.

heavy atom effect, consequently increasing the triplet state population. The conjugates displayed further increase in Φ_T (Table 1) compared to Pcs alone due to the presence of gold, a heavy atom as explained before. The AuNSs conjugates displayed higher Φ_T values than their corresponding AuNTs counterparts due to increased loading. The MPcs with the benzothiazole phenoxy groups (complexes **3** and **4**), displayed high Φ_T compared to the corresponding thiophene ethoxy groups (complexes **1** and **2**) suggesting that the former promotes intersystem crossing to the triplet state more than the latter. There was shortening of lifetimes for complexes **1** and **2** in the presence of the NPs, as expected since high Φ_T values are usually accompanied by short triplet lifetimes; however, this is not the case for complexes **3** and **4** (both with the benzothiazole phenoxy group) in the presence of NPs suggesting the protection of the complexes by the NPs. The lengthening of lifetimes for complexes linked to AuNTs when compared to AuNSs also suggest that the larger AuNTs (52.7 nm edge length) protected complexes more than the smaller AuNSs (15.2 nm). The Φ_T of the conjugates in water could not be obtained due to aggregation of phthalocyanines in water, however the reasonable high Φ_T in DMSO especially for complexes **3** and **4** in the presence of NPs makes them suitable for all applications that require a high Φ_T.

3.2.3. *Singlet oxygen quantum yields (Φ_Δ)*

Singlet oxygen is produced when the MPc in its excited triplet state transfers its energy to ground state molecular oxygen. This is quantitatively determined as the singlet oxygen quantum yield (Φ_Δ). Φ_Δ values were determined by monitoring the chemical photodegradation of the singlet oxygen quenchers; DPBF in DMSO (using **4**-AuNTs) and ADMA in water (using **1**-AuNSs) over a period of time (Fig. 9). In all complexes and conjugates studied, the Q-band remained unchanged, proving the stability over the irradiation period, while DPBF and ADMA degraded.

As expected, the Φ_Δ values (Table 1) followed the same trend observed for the Φ_T values, since singlet oxygen formation is dependent on the Φ_T value. The values in water are lower due to aggregation as shown by the broadening of the Q-band (Fig. S2). Water is known to quench the singlet state [56] mainly because

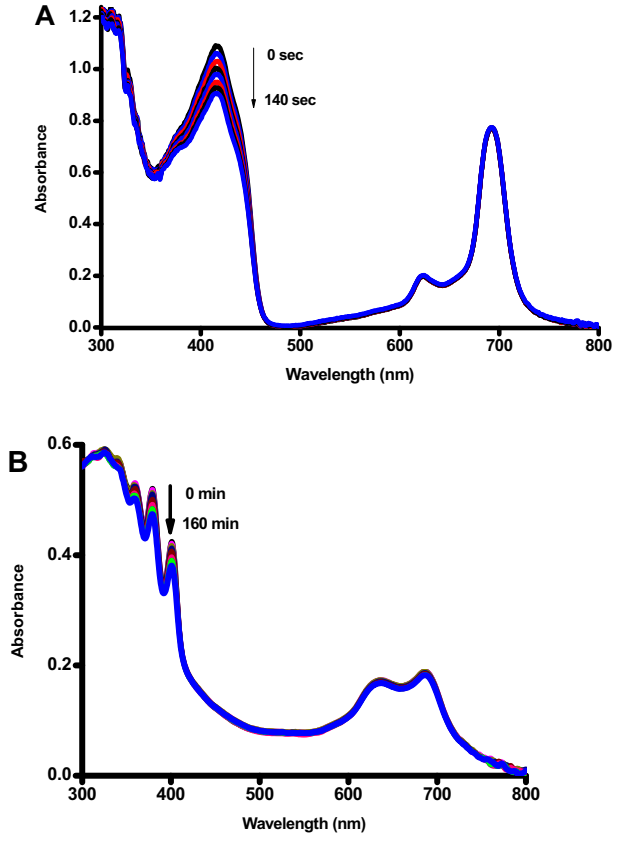

Fig. 9. The UV-Vis spectra showing the degradation of (A) DPBF in the presence of **4**-AuNTs in DMSO and (B) ADMA in the presence of **1**-AuNSs in water containing 1% (v/v) DMSO.

aggregation reduces the excited state lifetimes and the photosensitizing efficiency, due to enhanced radiationless decay which therefore lowers the quantum yields of the triplet excited states and hence the singlet oxygen generation. In addition, oxygen has higher solubility in many organic solvents compared to water [57], which could be responsible for low singlet oxygen generation in water.

The enhancement of the singlet oxygen quantum yield on conjugation shows that the Pc complexes may be used for photodynamic therapy in the presence of different shapes and sizes of AuNPs. PS such as lutetium texaphyrin with low Φ_Δ values in water (0.11) have been employed for clinical application in PDT [58], hence these conjugates can still be applicable in PDT.

4. Conclusion

Complexes **1**–**4** were linked to both AuNTs and AuNSs through S-Au (and N-Au for **3** and **4**) self-assembly. The formed conjugates were characterised using UV/vis absorption and emission spectrometer, XRD and EDX. The photophysicochemical behaviour of Pc complexes alone and their conjugates were studied. The conjugates displayed improved triplet and singlet quantum yields than complexes alone. On the other hand, the conjugates to nanospheres displayed improved triplet and singlet quantum compared to nanotriangles. The conjugates especially those with the benzothiazole phenoxy groups displayed Φ_Δ values in water $\geq$0.10, hence they have potential as PS for PDT applications.

Acknowledgements

This work was supported by the Department of Science and Technology (DST) Innovation and National Research Foundation (NRF), South Africa through DST/NRF South African Research Chairs Initiative for Professor of Medicinal Chemistry and Nanotechnology (UID 62620) as well as Rhodes University.

Appendix A. Supplementary data

Supplementary data to this article can be found online at https://doi.org/10.1016/j.molstruc.2018.12.091.

References

[1] R. Bonnett, In Chemical Aspects of Photodynamic Therapy, Gordon and Breach, Science Publishers, Amsterdam, 2000, p. 34.
[2] C.B. Silva, A.O. Ribeiro, H.P.M. de Oliveira, Solvent effect, photochemical and photophysical properties of phthalocyanines with different metallic Nuclei, Orbit. Electron. J. Chem. 9 (2017) 344–353.
[3] A. Nas, H. Kantekin, M. Durmus, N. Gumrukcuoglu, The influence of the various central metals on photophysical and photochemical properties of benzothiazole-substituted phthalocyanines, J. Lumin. 154 (2014) 15–21.
[4] P.C. Lo, S.Y.S. Chow, D.K.P. Ng, In Handbook of photodynamic therapy, in: P. Ravindra, D. Thomas J, Ke (Eds.), Updates on Recent Applications. Molecular Phthalocyanine- Based Photosensitizers for Photodyanic Therapy, 2016, pp. 237–272.
[5] R. R Allison, G. H Downie, R. Cuenca, X.H. Hu, C.J. H Childs, S. Claudio, Photosensitizers in clinical PDT, Photodiagn. Photodyn. Ther. 1 (2004) 27—42.
[6] R. W Boyle, D. Dolphin, Structure and biodistribution relationships of photodynamic sensitizers, Photochem. Photobiol. 64 (1996) 469–485.
[7] S.B. Brown, E.A. Brown, I. Walker, The present and future role of photodynamic therapy in cancer treatment, Lancet Oncol. 5 (2004) 497–508.
[8] U. Chitgupi, Y. Qin, J.F. Lovell, Targeted nanomaterials for phototherapy, Nanotheranostics 1 (2017) 38–58.
[9] E.J. Hong, D.G. Choi, M.S. Shim, Targeted and effective photodynamic therapy for cancer using functionalized nanomaterials, Acta Pharm. Sin. B. 6 (2016) 297–307.
[10] K. Greish, Enhanced permeability and retention (EPR) effect for anticancer nanomedicine drug targeting, in: S. Grobmyer, B. Moudgil (Eds.), Cancer Nanotechnology. Methods Mol Biol. (Methods and Protocols) vol. 624, Humana Press, 2010, pp. 25–37.
[11] J. Fang, H. Nakamura, H. Maeda, The EPR effect: unique features of tumor blood vessels for drug delivery, factors involved, and limitations and augmentation of the effect, Adv. Drug Deliv. Rev. 63 (2011) 136–151.
[12] D.K. Chatterjee, L.S. Fong, Y. Zhang, Nanoparticles in photodynamic therapy: an emerging paradigm, Adv. Drug Deliv. Rev. 60 (2008) 1627–1637.
[13] G. Obaid, M. Broekgaarden, A.L. Bulin, H.C. Huang, J. Kuriakose, J. Liu, T. Hasan, Photonanomedicine: a convergence of photodynamic therapy and nanotechnology, Nanoscale 8 (2016) 12471–12503.
[14] S. Kapse-Mistry, T. Govender, R. Srivastava, M. Yergeri, Nanodrug delivery in reversing multidrug resistance in cancer cells, Front. Pharmacol. 5 (2014) 159 (22 Pages).
[15] L. Illum, S.S. Davis, C.G. Wilson, N.W. Thomas, M. Frier, J.G. Hardy, Blood clearance and organ deposition of intravenously administered colloidal particles - the effects of particle-size, nature and shape, Int. J. Pharm. 12 (1982) 135–146.
[16] R. Toy, P.M. Peiris, K.B. Ghaghada, E. Karathanasis, Shaping cancer nanomedicine: the effect of particle shape on the in vivo journey of nanoparticles, Nanomedicine 9 (2014) 121–134.
[17] B.D. Chithrani, W.C. Chan, Elucidating the mechanism of cellular uptake and removal of protein-coated gold nanoparticles of different sizes and shapes, Nano Lett. 7 (2007) 1542–1550.
[18] M. Caldorera-Moore, N. Guimard, L. Shi, K. Roy, Designer nanoparticles: incorporating size, shape, and triggered release into nanoscale drug carriers, Expert Opin. Drug Deliv. 7 (2010) 479–495.
[19] N.P. Truong, M.R. Whittaker, C.W. Mak, T.P. Davis, The importance of nanoparticle shape in cancer drug delivery, Expert Opin. Drug Deliv. 12 (2015) 129–142.
[20] X. Xie, J. Liao, X. Shao, Q. Li, Y. Lin, The effect of shape on cellular uptake of gold nanoparticles in the forms of stars, rods, and triangles, Sci. Rep. 7 (2017) 3827, 9 pages.
[21] K.N. Solovev, E.A. Borisevich, Intramolecular heavy-atom effect in the photophysics of organic molecules, Phys. Usp. 48 (2005) 231–253.
[22] C.G. Mortimer, G. Wells, J.F. Crochard, E.L. Stone, T.D. Bradshaw, M.F.G. Stevens, A.D. Westwell, Antitumor benzothiazoles. 26. 2-(3,4-Dimethoxyphenyl)-5-fluorobenzothiazole (GW 610, NSC721648), a simple fluorinated 2-arylbenzothiazole, shows potent and selective ınhibitory activity against lung, colon, and breast cancer cell lines, J. Med. Chem. 49 (2006) 179–185.
[23] D. Havrylyuk, L. Mosula, B. Zimenkovsky, O. Vasylenko, A. Gzella, R. Lesyk, Synthesis and anticancer activity evaluation of 4-thiazolidinones containing benzothiazole moiety, Eur. J. Med. Chem. 45 (2010) 5012–5021.
[24] P.C. Sharma, A. Sinhmar, A. Sharma, H. Rajak, D.P. Pathak, Medicinal significance of benzothiazole scaffold: an insight view, J. Enzym. Inhib. Med. Chem. 28 (2013) 240–266.
[25] K.S. Rakesh, S. Jagadish, T.R. Swaroop, C.D. Mohan, N. Ashwini, K.B. Harsha, F. Zameer, K.S. Girish, K.S. Rangappa, Anti-cancer activity of 2,4-disubstituted thiophene derivatives: dual inhibitors of lipoxygenase and cyclooxygenase, Med. Chem. 11 (2015) 462–472.
[26] F.A. Dos Santos, M.C. Pereira, T.B. de Oliveira, F.J.B. Mendonca Junior, M.D.C.A. de Lima, M.G.D.R. Pitta, I.D.R. Pitta, M.J.B. de Melo Rego, M.G. da Rocha Pitta, Anticancer properties of thiophene derivatives in breast cancer MCF-7 cells, Anti Canccer Drugs 29 (2018) 157–166.
[27] J. Obirai, T Nyokong Synthesis, Electrochemical and electrocatalytic behaviour of thiophene-appended cobalt, manganese and zinc phthalocyanine complexes, Electrochim. Acta 50 (2005) 5427–5434.
[28] E. Dube, D.O. Oluwole, T. Nyokong, Improved photophysical and photochemical properties of thiophene-ethoxy substituted metallophthalocyanines on immobilization onto gold-speckled silica nanoparticles, Photochem. Photobiol. 94 (2018) 521–553.
[29] A. Aktas, M. Durmus, L. Degrmencioglu, Self-assembling novel phthalocyanines containing a rigid benzothiazole skeleton with a 1,4-benzene linker: synthesis, spectroscopic and spectral properties, and photochemical/photophysical affinity, Polyhedron 48 (2012) 80–91.
[30] N. Nwaji, B. Jones, J. Mack, D.O. Oluwole, T. Nyokong, Nonlinear optical dynamics of benzothiazole derivatized phthalocyanines in solution, thin films and when conjugated to nanoparticles, J. Photochem. Photobio. A Chem. 346 (2017) 46–59.
[31] N. Masilela, T. Nyokong, Conjugates of low-symmetry Ge, Sn and Ti carboxy phthalocyanines with glutathione caped gold nanoparticles: an investigation of photophysical behaviour, J. Photochem. Photobiol. Chem. 223 (2011) 124–131.
[32] L. Chen, F. Ji, Y. Xu, L. He, Y. Mi, F. Bao, B. Sun, X. Zhang, Q. Zhang, High-yield seedless synthesis of triangular gold nanoplates through oxidative etching, Nano Lett. 14 (2014) 7201–7206.
[33] T.H. Tran-Thi, C. Desforge, C. Thiec, S.J. Gaspard, Singlet–singlet and triplet–triplet intramolecular transfer processes in a covalently linked porphyrin–phthalocyanine heterodimer, J. Phys. Chem. 93 (1989) 1226–1233.
[34] A. Ogunsipe, J.Y. Chen, T. Nyokong, Photophysical and photochemical studies of zinc (II) phthalocyanine derivatives– effects of substituents and solvents, New J. Chem. 28 (2004) 822–827.
[35] N.A. Kuznetsova, N.S. Gretsova, O.A. Yuzhakova, V.M. Negrimovskii, O.L. Kaliya, E.A. Luk'yanets, New reagents for determination of the quantum efficiency of singlet oxygen generation in aqueous media, Russ. J. Gen. Chem. 71 (2001) 36–41.
[36] W. Spiller, H. Kliesch, D. Wohrle, S. Hackbarth, B. Roder, G. Schnurpfeil, Singlet

oxygen quantum yields of different photo-sensitizers in polar solvents and micellar solutions, J. Porphyr. Phthalocyanines 2 (1998) 145–158.
[37] T. Nyokong, E. Antunes, Photochemical and photophysical properties of metallophthalocyanines, in: K.M. Kadish, K.M. Smith, R. Guilard (Eds.), The Handbook of Porphyrin Science, World Scientific, Singapore, 2010, pp. 247–349.
[38] J.E. Millstone, S. Park, K.L. Shuford, L. Qin, G.C. Schatz, C.A. Mirkin, Observation of a quadrupole plasmon mode for a colloidal solution of gold Nanoprisms, J. Am. Chem. Soc. 127 (2005) 5312–5313.
[39] M.J. Stillman, T. Nyokong, in: C.C. Leznoff, A.B. P Lever (Eds.), Phthalocyanines: Properties and Applications, vol. 1, VCH Publishers, New York, NY, 1989 (Chapter 3).
[40] E. Gurel, M. Pişkin, S. Altun, Z. Odabaş, M. Durmuş Synthesis, Characterization and investigation of the photophysical and photochemical properties of highly soluble novel metal-free, zinc(II), and indium(III) phthalocyanines substituted with 2,3,6-trimethylphenoxy moietie, Dalton Trans. 44 (2015) 6202–6211.
[41] L. Li, J.F. Zhao, N. Won, H. Jin, S. Kim, J.Y. Chen, Quantum dot - aluminum phthalocyanine conjugates perform photodynamic reactions to kill cancer cells via fluorescence resonance energy transfer (FRET), Nanoscale Res. Lett. 7 (2012) 386–393.
[42] Y. Bae, N.H. Kim, M. Kim, K.Y. Lee, S.W. Han, Anisotropic assembly of Ag Nanoprisms, J. Am. Chem. Soc. 130 (2008) 5432–5433.
[43] A. Nagal, R. K Singla, Nanoparticles in different delivery systems: a brief review, Indo Global J. Pharmaceut. Sci. 3 (2013) 96–106.
[44] E.M. Hotze, T. Phenrat, G.V. Lowry, Nanoparticle aggregation: challenges to understanding transport and reactivity in the environment, J. Environ. Qual. 39 (2010) 1909–1924.
[45] M.H. Majles Ara, Z. Dehghani, R. Sahraei, A. Daneshfar, Z. Javadi, F. Divsar, Diffraction patterns and nonlinear optical properties of gold nanoparticles, J. Quant. Spectrosc. Radiat. Transfer 113 (2012) 366–372.
[46] R. Prabakaran, R. Kesavamoorthy, G.L.N. Reddy, F.P. Xavier, Structural investigation of copper phthalocyanine thin films using X-ray diffraction, Raman scattering and optical absorption measurements, Phys. Status Solidi 229 (2002) 1175–1186.
[47] R. Jenkins, R.L. Synder, Introduction to X-ray Diffractometry, vol. 138, Wiley and Sons, New York, 1996.
[48] C. Xue, Y. Xue, L. Dai, A. Urbas, Q. Li, Size and shape-dependent fluorescence quenching of gold nanoparticles on perylene dye, Adv. Opt. Mater. 1 (2013) 581–587.
[49] J.A. Lacey, D. Philips, Fluorescence lifetime measurements of disulfonated aluminium phthalocyanine in the presence of microbial cells, Photochem. Photobiol. Sci. 1 (2002) 378–383.
[50] J. Kümmerlen, A. Leitner, H. Brunner, F.R. Aussenegg, A. Wokaun, Enhanced dye fluorescence over silver island films: analysis of the distance dependence, Mol. Phys. 80 (1993) 1031–1046.
[51] C.D. Geddes, in: J.R. Lakowicz (Ed.), Topics in Fluorescence Spectroscopy, Springer, New York, 2005.
[52] G.D.C. Naulin, M. Costes, A. Benseddick, Kinematic effects on laser-induced fluorescence measurements performed in reactive crossed beam experiments, Laser Chem. 8 (1988) 238–302.
[53] D. Phillips, A lifetime in photochemistry; Some ultrafast measurements on singlet states, Proc. Roy. Soc. A Math. Phys. Eng. Sci. 472 (2016), 20160102 (21 pages).
[54] Z.N. Erol, P. Atienzar, Y. Arslanoglu, E. Hamuryudan, H. García, Synthesis and photophysical properties of phthalocyanines having calixpyrrole units, RSC Adv. 5 (2015) 55901–55908.
[55] M.G. Debacker, O. Deleplanque, B. Van Vlierberge, F.X. Sauvage, A laser photolysis study of triplet lifetimes and of triplet–triplet annihilation reactions of phthalocyanins in DMSO solutions, Laser Chem. 8 (1988) 1–11.
[56] A.B. Ormond, H.S. Freeman, Dye sensitizers for photodynamic therapy, Materials 6 (2013) 817–840.
[57] H. Ramesh, T. Mayr, M. Hobisch, S. Borisov, I. Klimant, U. Krühne, J.M. Woodley, Measurement of oxygen transfer from air into organic solvents, J. Chem. Technol. Biotechnol. 91 (2016) 832–836.
[58] J.L. Sessler, W.C. Dow, D.O. Connor, A. Harriman, G. Hemmi, T.D. Mody, R.A. Miller, F. Qing, S. Springs, K. Woodburn, S.W. Young, Biomedical applications of lanthanide (III) texaphyrins Lutetium(III) texaphyrins as potential photodynamic therapy photosensitizers, J. Alloy. Comp. 249 (1997) 146–152.